ALTERNATIVE MICROMACHINING APPROACHES FOR THE REALIZATION OF ROBUST MEMS

Mark G. Allen and Ari Glezer
Georgia Institute of Technology

ABSTRACT

This work describes efforts in the fabrication and testing of robust microelectromechanical systems (MEMS). Robustness is typically achieved by investigating non-silicon substrates and materials for MEMS fabrication. Some of the traditional MEMS fabrication techniques are applicable to robust MEMS, while other techniques are drawn from other technology areas, such as electronic packaging. The fabrication technologies appropriate for robust MEMS are illustrated through three examples: wireless micromachined ceramic pressure sensors for high temperature application in turbine compressors; micromachined stainless steel pressure sensor arrays; and micromachined stainless steel modulators for synthetic jets intended for aerodynamic control applications.

INTRODUCTION

Microelectromechanical systems (MEMS) have been primarily realized using silicon substrates. In many applications, the use of traditional silicon-substrate micromachined devices may be limited, for example by the lack of ability of the surrounding silicon substrate to absorb large mechanical shocks. In this work, we have investigated the use of more robust substrates as suitable starting points for both bulk and surface micromachined structures, as well as investigated the possibility of the substrate forming essential structural components of the device package. Alternative fabrication techniques, such as techniques more commonly used in either conventional machining as well as electronic packaging fabrication (e.g., lamination), are combined with more traditional integrated-circuit-based microelectronics processing techniques to create micromachined devices on or from these robust substrates.

One of the advantages of the use of robust substrates is the possibility of co-fabrication of the micromachined devices and their packages using, e.g., the robust substrate itself as an integral part of the sensor package. Another advantage is that due to substrate robustness, these co-packaged devices may be able to be used in mechanically harsh environments, such as high temperature and/or aerodynamic applications. Finally, it is envisioned that the larger-scale devices (especially actuators) producible by this fabrication technology will have increased control authority over their silicon counterparts.

Fabrication technologies for robust MEMS are illustrated in this paper by way of three examples: wireless micromachined ceramic pressure sensors for high temperature application in turbine compressors; micromachined stainless steel pressure sensor arrays; and micromachined stainless steel modulators for synthetic jets intended for aerodynamic control applications. Each of these is described in detail below.

Mark G. Allen is Professor of Electrical and Computer Engineering, Georgia Institute of Technology, Atlanta.

Ari Glezer is Professor of Mechanical Engineering, Georgia Institute of Technology, Atlanta, and a Member of the AIAA.

HIGH TEMPERATURE CERAMIC PRESSURE SENSORS

Micromachined silicon pressure sensors are widely utilized in industry. In general, the pressure sensor design is based on a flexible silicon membrane as the sensing element, coupled with silicon piezoresistors or a capacitive structure and silicon circuitry for data retrieval. These sensors are well developed and have been documented extensively in the literature [1]. However, micromachined silicon sensors are typically subject to operating temperature limitations due to a variety of factors, including piezoresistive temperature sensitivity and the poor mechanical properties of silicon at higher temperatures. Thus, applications such as sensing pressure in turbine engine compressors require development of other types of sensors that offer high temperature stability.

In the literature, potential high-temperature materials have been investigated as an alternative to silicon processing. Silicon carbide, polycrystalline diamond and ceramic materials have been reported as high-temperature materials for sensor fabrication [2-3]. Silicon carbide pressure sensors employ the flexible membrane design and use piezoresistors to measure pressure changes. Silicon carbide circuitry is also possible to retrieve the pressure data. Polycrystalline diamond pressure sensors also employ a flexible membrane and piezoresistors. These technologies show great promise for integrated high temperature pressure sensors, but their manufacturing infrastructure is not nearly as well developed as that for silicon and electronic packages for silicon.

The microelectronics packaging industry offers a well-developed ceramic packaging procedure using ceramic co-fireable tape. The ceramic tape consists of alumina particles and glass particles suspended in an organic binder, which is subsequently fired to form a ceramic structure. In general, this type of tape is referred to as low temperature co-fireable ceramic (LTCC) as the curing (firing) temperature is 900°C [4]. Ceramic tapes made solely from alumina particles are also available and have curing temperatures above 1600°C. Besides high temperature stability, the co-fired ceramic tape has good mechanical properties that allow similar membrane designs as the silicon pressure sensors. From our investigations, the ceramic tape is an excellent choice for the fabrication of pressure sensors for high temperatures.

Background - Ceramic Fabrication

The microelectronics packaging infrastructure has developed ceramic multi-layer multi-chip modules as a means of complex packaging. A simple diagram of this procedure is given in Figure 1. The layers of ceramic tape are punched to form vias and are metallized to form conductor lines. The layers are then aligned and laminated together in a hot press. The package is fired in a furnace to bake off the organics and form the final package. Circuit chips are then soldered to the metal pads of the package. The co-fired ceramic tape and the processing procedures developed by the microelectronics packaging infrastructure can be used to fabricate a pressure sensor. A slight modification of these standard techniques allows the creation of a thin flexible membrane that can sense pressure. In addition, ceramic packaging technology allows for the embedding of integrated passive elements (resistors, inductors, and capacitors) in the body of the package itself, which will be used for passive wireless communication as described below.

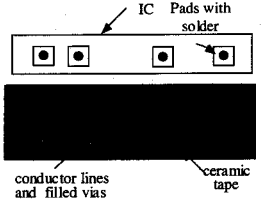

Figure 1. *Simplified schematic of multilayer tape-based ceramic package.*

Conventional micromachined pressure sensors depend on some type of interface with the sensing element (i.e. flexible diaphragm, piezoresistors, and capacitive elements) to read

out the pressure data. This interface can be, e.g., silicon circuitry and wire leads, or an optical interface. These readout methods may be infeasible for high temperature or harsh environments or environments where it is difficult to physically connect wires or other interfaces to the sensor. Recognizing that at extremely high operating temperatures, simplicity of the sensor is desirable, a completely passive, wireless telemetry system that requires no physical contact with the sensor and no active elements such as power supplies, transistors, or batteries, is employed.

A schematic of the wireless pressure sensor concept is shown in Figure 2. The sensor consists of a sealed cavity, ideally containing vacuum, on which two capacitor plates are formed. If either the top or the bottom (or both) bounding sides of the cavity are made of a flexible ceramic diaphragm, the value of this capacitor will change with pressure. In order to measure this capacitance change, a resonant technique is employed, in which a planar spiral inductor coil fabricated using ceramic-based integral passives techniques is electrically connected to the capacitor. These components form a passive resonant LC circuit, where the resonant frequency is given by [5]:

$$f_o = \frac{1}{2\pi\sqrt{L \bullet C(P)}} \qquad (1)$$

Thus, as the external pressure increases, the capacitance increases and the resonant frequency of the LC circuit will decrease.

To achieve passive wireless telemetry, the circuit is placed in proximity to an external loop antenna coil and the impedance and phase response of the antenna coil are monitored as a function of frequency by an impedance meter. At frequencies far from the sensor frequency (and below the self-resonant frequency of the antenna itself), the antenna appears as an inductance, with a rising impedance response with frequency and a phase shift of +90 degrees. At the sensor resonant frequency, the antenna impedance decreases and the phase response of the antenna to drops from +90 degrees.

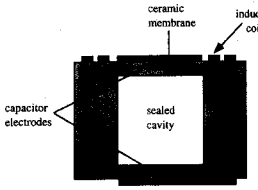

Figure 2. *Pressure sensor concept.*

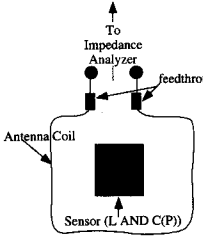

Figure 3. *Wireless passive telemetry for pressure sensing.*

Although the magnitude of the phase peak depends upon the details of the specific sensor-to-antenna coupling, there are configurations in which the peak position (i.e., frequency) dependencies are negligible. Thus, this wireless data retrieval scheme could also work for a sensor in motion within the antenna (e.g. mounted on a moving part). In addition, it is possible to have an array of such sensors, with each sensor designed to have a distinct 'center' frequency (i.e., frequency given by equation (1) under zero applied pressure), with the number of such sensors limited by the available frequency bandwidth.

Pressure Sensor Design and Fabrication

The design of the sensor involves the creation of the flexible membrane, the sealed cavity and the integration of the LC resonant circuit. The basic structure and assembly is shown in Figure 4. To create the flexible membrane, sealed cavity, and ultimately the capacitor, a three-layer structure is required. The first layer, which becomes the flexible membrane, consists of one sheet of ceramic tape (Figure 4(a)). The second layer consists of at least one sheet of ceramic tape with a hole punched into it. Finally, the third layer consists of at least one sheet of ceramic tape. By increasing the number of sheets of ceramic tape in the third layer, the layer becomes less flexible and less sensitive to pressure. The layers are aligned and laminated together in a hot vacuum press and fired in a furnace (Figure 4(b)). The final structure is shown in Figure 4(c).

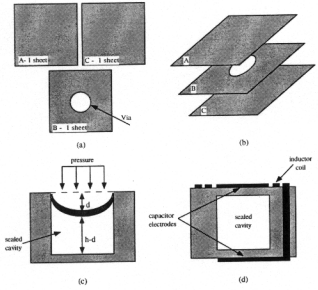

Figure 4. *Diagram of basic concept structure. (a) 3 layers of ceramic tape, (b) assembly and lamination of 3 layers, (c) final package. (d) sensor design concept*

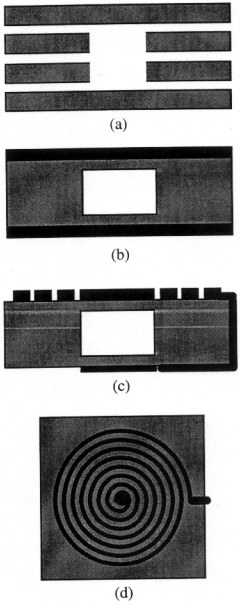

Figure 5. *Ceramic micromachined pressure sensor fabrication. (a) ceramic tape layers punched and aligned. (b) after lamination, firing and metallization. (c) after electroplating coil and electrodes. (d) top view of wireless ceramic pressure sensor.*

The sensor is fabricated using 4 sheets of Dupont 951AT ceramic tape [4]. The tape consists of alumina and glass particles suspended in an organic binder. Each sheet is cut to a size of 2.5 inch square with a thickness of ~100μm each. Of the four sheets, two are punched to create the via for the sealed cavity. The diameter of the via is 7.6mm. The four layers are aligned in a press mold that consists of two aluminum plates that are 2.5 inches square and 0.25 inches thick. The ceramic sheets are laminated together in a hot vacuum press for 10 minutes at a press temperature of 70°C and a press force of 9.38 tons under ambient vacuum. After lamination, the sample is cut down to a 1.5 inch square before firing. The sample is fired in a box furnace in air for 30 minutes at 500°C to bake off the organics and then for 20 minutes at 850°C to melt the glass particles and harden the sample.

To create the LC circuit, the top side of the sensor is DC sputtered with an electroplating seed layer of 500Å of titanium followed by 3600Å of copper. Shipley 5740 photoresist is used to create a plating mold that will define the inductor coil and one electrode of the parallel plate capacitor. Using a copper electroplating bath, copper is electroplated onto the seed layer to a thickness of ~28μm and the plating mold and seed layer are removed using wet etching. On the back side of the sensor, the other electrode of the capacitor is patterned using a DC sputtered titanium/copper layer sputtered through a shadow mask. Contact from the outer arm of the inductor coil on the top side of the sensor to the capacitor electrode on the back side is made using Dupont 6160 silver-filled external conductor paste for co-fireable tapes. A diagram of the fabrication process is given in Figure 5. A picture of the fabricated sensor is given in Fig. 6.

Sensor Operation

A diagram of the wireless ceramic pressure sensor test setup is given in Figure 7. The sensor is placed in a pressure and temperature varying chamber. An antenna coil is placed in the chamber in proximity the sensor and connected to an impedance meter via feedthroughs from the chamber. The impedance meter reads the phase value of the antenna coil over the frequency range. At atmospheric pressure, the phase of the antenna is +90° except at the resonant frequency of the sensor. At the resonant frequency, the capacitor of the sensor couples to the antenna coil and causes a dip in the phase from +90°. As the chamber pressure increases, the ceramic membrane will deflect causing an increase in the sensor capacitance and a decrease in the resonant frequency and thus, the dip the phase will shift down in the frequency range.

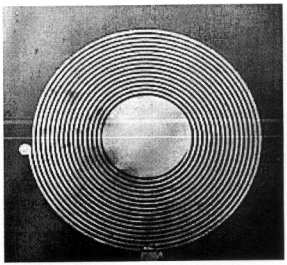

Figure 6. *Photomicrograph of a typical micromachined ceramic pressure sensor.*

Wireless pressure and temperature tests were performed using an HP4194A impedance analyzer, a Parr 4570 pressure vessel for high pressure tests, and a VWR vacuum oven for low pressure and temperature tests. Figure 8 shows the raw data obtained, phase versus frequency, for zero and full-scale (1 bar) applied pressure for a single sensor. In Figure 9, the raw data of Figure 8 is shown for a variety of pressures between 0 and 1 bar, at 25°C and 200°C. Figure 10 shows the high pressure (0-100 bar) response of the sensor. In Figure 11, the sensor array concept is demonstrated for three sensors.

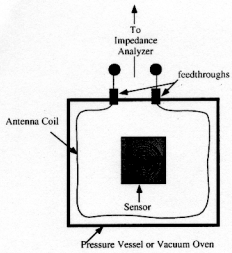

Figure 7. *Diagram of test setup.*

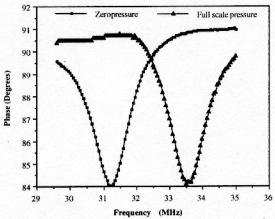

Figure 8. *Phase versus frequency for zero and full scale applied pressure (0-1bar).*

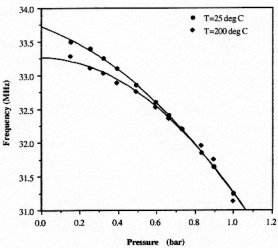

Figure 9. *Frequency versus pressure for 25°C (upper curve) and 200°C (0-1bar)*

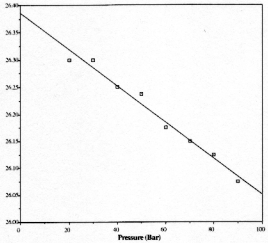

Figure 10. *Frequency versus pressure for the high pressure range (0-100bar)*

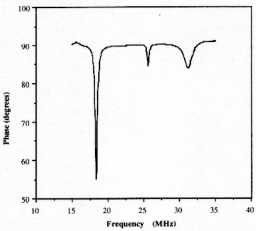

Figure 11. *Simultaneous data logged from three sensors within a single loop antenna. Each sensor is designed to have a distinct center frequency, thereby allowing simultaneous readout.*

For the results in Figures 8 and 9, the pressure sensor was designed to have an electrode radius of 5mm, a membrane thickness of 96μm, and an effective electrode gap of 217μm. The sensitivity of the sensor was calculated from the measure data to be 2.6MHz/bar. The same sensor was tested at 25°C and 200°C and except at low pressures, little difference is seen in

sensor performance between the two temperatures. Higher temperatures may have a more significant effect. For the results in Figure 10, the pressure sensor was designed to have an electrode radius of 3.8mm, a membrane thickness of 96μm, and an effective electrode gap of 217μm. This sensor was subjected to a much larger pressure range (0-100 bar) and because of this the sensor electrodes were designed to be smaller. The sensitivity, calculated from the measured data is S=6.4kHz/bar. The reduced sensitivity is due to the fact that the sensor membrane deflection is equal to the electrode gap (i.e. the membrane has made contact to the lower electrode). This can be avoided by making the membrane radius larger and/or by making the electrode gap larger.

Figure 11 illustrates the array concept. Three sensors were tested simultaneously using the same antenna coil. Each sensor was designed for a different center frequency. The variation in peak height for the three sensors reflects different degrees of sensor/antenna coupling (i.e. proximity of the sensor to the antenna coil). However, to determine pressure, only the peak position is required. Since each sensor has a different carrier frequency and thus a different frequency shift due to pressure, each sensor can be monitored simultaneously by tuning into a particular sensors frequency band.

Pressure Sensor Modeling

Theoretical models for deflection of circular diaphragms and the associated capacitance were used to model and predict the behavior of the sensor. It is assumed, for this analysis, that only one membrane of the sensor deflects. For a clamped circular plate that is subjected to both stretching and bending, the deflection is given by

$$d_o = \frac{Pa^4}{Et^3} \cdot \frac{1}{1 + .488\left(d_o/t\right)^2} \qquad (2)$$

where d_o is the deflection of the plate, a is the radius of the plate, t is the thickness of the plate, E is the Young's modulus, and P is the applied pressure [6]. Using this equation, the amount of deflection for applied pressure is predicted. To determine the change in capacitance as a function of the deflection, a model given by:

$$\frac{C_+}{C_o} = \sum_{i=0}^{\infty} \frac{1}{2+1}\left(\frac{d_o}{h}\right)^i \qquad (3)$$

was used (see p. 9). In this equation, do is the deflection determined from the deflection equation and h is the electrode gap. The resonant frequency was determined using:

$$f = \frac{f_o}{\sqrt{C_+/C_o}} \qquad (4)$$

where f_o is the measured resonant frequency at 0 bar. The measured resonant frequency is used instead of the calculated resonant frequency because the calculated resonant frequency does not allow for the parasitic capacitances associated with the windings of the inductor coil and the conductive paste that connects the inductor to the capacitor.

A plot of the predicted behavior and the measured data of the sensor, resonant frequency versus pressure (0-1 bar) is given in Figure 12. The sensor was modeled to have the same design elements as the fabricated sensor tested in Figures 8 and 9. The sensitivity of the pressure sensor was calculated to be 2.2 MHz/bar. A comparison of the theoretical data to the experimental data shows similar behavior. The differences between the sensitivities the model and the actual sensor are due to the fact that some deflection of the bottom plate occurs which allows for the increase in the sensitivity of the sensor to 2.6MHz/bar.

Summary – Ceramic Pressure Sensors

The design, modeling, fabrication and testing of a wireless ceramic sensor are presented. The sensor is made from ceramic co-fired tape to create a sealed cavity structure with a flexible ceramic membrane. The ceramic structure is integrated with a varying C/fixed L resonant circuit. The resonant frequency of the sensor will shift with applied pressure. Results of pressure and temperature tests are presented and

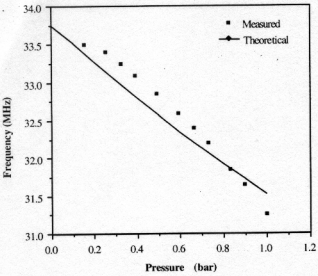

Figure 12. *Comparison of theoretical to actual pressure data.*

show that this concept is valid. The theoretical model compares well the measured data where the theoretical sensitivity is 2.2MHz/bar and the measured sensitivity is 2.6MHz/bar. The sensor array concept is also demonstrated.

LAMINATED STAINLESS STEEL PRESSURE SENSORS

Since the historic root of micromachining technology is in integrated circuit processing technology, micromachined devices have been primarily realized using silicon substrates. In many applications, the use of traditional silicon-substrate micromachined devices may be limited, for example by the lack of ability of the surrounding silicon substrate to absorb large mechanical shocks. In this work, robust substrates, such as stainless steel, have been studied as substrates for micromachined devices. The use of robust substrates may allow for the co-fabrication of micromachined devices and sensor packages. Lamination process techniques combined with traditional micromachining processes have been investigated as suitable fabrication technologies. To illustrate these principles, a capacitive pressure sensor array has been designed, fabricated, and characterized using a stainless steel substrate, Kapton polyimide film or patterned stainless steel diaphragms as a suspended movable plate, and an electroplated nickel fixed back electrode. The net capacitance change of this sensor over the applied pressure range (0 to 34 kPa) was approximately 0.14 pF. Multivibrator circuitry has been integrated with pressure sensors in a hybrid fashion and used for frequency-modulated output measurements. An important attribute of this design is that only the steel substrate and the pressure sensor inlet is exposed to the flow; i.e., the sensor is self-packaged.

Theory and Design

The sensor device concept is based on the pressure-induced deflection of a metallized flexible plate and the subsequent measurement of the capacitance between this deflecting plate and a fixed backplate surface micromachined over the deflecting plate.

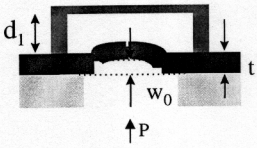

Figure 13. *A schematic diagram of the side-view of the capacitive pressure sensor.*

Figure 13 shows a schematic diagram of the side-view of the device, where d_1 is an initial (undeflected) gap distance between the fixed back electrode and the flexible plate electrode, w_o is the deflection at the center of the plate, t is the thickness of the plate, and P is the uniform applied pressure. For analytical modeling [6], several assumptions have been made: (a) stretching of the plate has been neglected, since the plate will not be undergoing deflections large compared with its thickness; (b) the thickness of the metallic electrode on the plate has been neglected, since this thickness is small compared with the plate thickness; (c) residual stress in the plate has been neglected, since (as will be

discussed later) the plate is formed using lamination; and (d) electric field fringing effects have been neglected, since the gap between the flexible plate and the fixed backplate is small compared with their lateral extents. Under these conditions, the deflection of a circular plate with fully clamped perimeter as a function of radius, $w(r)$, is given by:

$$w(r) = w_0\left[1-\left(\frac{r}{a}\right)^2\right]^2 \quad . \qquad (5)$$

where a is the radius of the plate ($0 \le r \le a$) and the deflection at the center of the plate w_0 is given by:

$$w_0 = \frac{Pa^4}{64D} \quad . \qquad (6)$$

In equation (6), D is the flexural rigidity of the plate which is given by:

$$D = \frac{Et^3}{12\left(1-\nu^2\right)} \quad . \qquad (7)$$

where E is the elastic modulus and ν is the Poisson ratio of the plate. The resultant sensor capacitance can be obtained by integration:

$$C_{sensor} = \varepsilon_0 \int_0^{2\pi} \int_0^a \frac{r dr d\theta}{\left(d_1 - w(r)\right)} \quad . \qquad (8)$$

Equation (8) can be nondimensionalized by substituting $x=r/a$, $\gamma=w_0/d_1$, and $f(\xi)=(1-\xi^2)^2$, yielding:

$$C_{sensor} = 2C_0 \int_0^1 \frac{\xi d\xi}{1-\gamma \bullet f(\xi)} \quad . \qquad (9)$$

where C_0 is the capacitance when the plate is undeflected. In equation (9), since $f(\xi)$ is bounded between zero and one, and γ is by definition less than one, the integrand can be expressed as a Taylor series expansion and the solution of equation (9) can be described as follows:

$$C_{sensor} = C_0\left(1 + K_1 P + K_2 P^2 + \cdots\right) \quad . \qquad (10)$$

where K_n are constants given by:

$$K_n = \frac{1}{(2n+1)}\left[\frac{a^4}{64Dd_1}\right]^n \quad , \qquad (11)$$

for $n \ge 1$.

Fabrication

The fabrication sequence of the robust capacitive pressure sensor array is shown in Figure 14. The process starts on square 5.7 cm (2 ¼ inch) on a side, 0.5 mm thick stainless steel substrates. An array of 8x8 pressure inlet holes with a diameter of 2mm, with 5mm center-to-center distances, are milled through the stainless steel substrate. Kapton polyimide film (Dupont, Kapton HN200, 50μm thick) is laminated onto the milled stainless steel substrate using a hot press. The pressure sensitive flexible plates will be the Kapton polyimide film in the regions suspended over the milled pressure inlet holes.

A triple metallic layer of Ti/Cu/Ti with a thickness of 100/2,000/500 Å is deposited on the surface of the Kapton polyimide film by electron-beam evaporation and then patterned to create bottom electrodes, electroplating seed layers, and bonding pads with a lift-off process (Figure 14a and Figure 15). Multiple layers of PI2611 polyimide (Dupont) are spun onto the patterned layer with a spin speed of 1,200 rpm for 60 seconds, and hard-cured in a N_2 ambient at 300 ^{o}C yielding a final thickness of polyimide of approximately 44~48 μm.

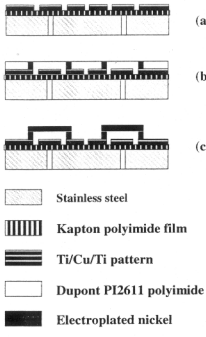

Figure 14. *Fabrication sequence: (a) lamination of milled stainless steel and Kapton polyimide film and bottom electrode patterning; (b) polyimide deposition and electroplating of nickel posts; (c) backplate electroplating and removal of polyimide sacrificial layer.*

The polyimide layer is anisotropically etched using reactive ion etching to create electroplating molds for the support posts of the fixed backplates, and to remove the uppermost titanium layer of the seed layer. Nickel supports are then electroplated through the polyimide molds (Figure 14b). A Ti/Cu/Ti metallic triple layer with a thickness of 300/2,000/300 Å is deposited using DC sputtering to act as a seed layer for the deposition of the backplate. Thick photoresist (Shipley PR 5740) is spun on the seed layer with a spin speed of 1,100 rpm for 30 seconds (yielding a final thickness of approximately 15 μm) and patterned to act as electroplating molds for the backplates. After removal of the uppermost Ti layer, nickel is electroplated through the thick photoresist electroplating molds to create the backplates. The thick photoresist electroplating molds and the remaining seed layer is removed. Finally, the polyimide molds for the backplate posts as well as polyimide sacrificial layers are isotropically etched to create air gaps between the fixed backplates and the pressure sensitive Kapton polyimide flexible plates (Figure 14c and Figure 16). The isotropic dry etch is carried out in a barrel plasma etcher using CF_4/O_2 plasma with a RF power of 120W. Figure 16 shows photographs of a fabricated pressure sensor array, where (a) shows a side-view and (b) shows a close-up view of the gap defined between the fixed backplate and the flexible plate.

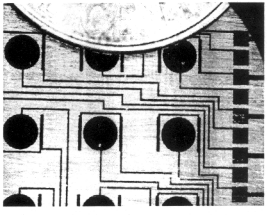

Figure 15. *A photograph of top-view of the metallic seed layer which corresponds to the fabrication sequence shown in Figure 2 (a). The pressure-sensitive flexible plates are located underneath the circular metallic patterns.*

(a)

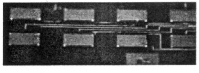

(b)

Figure 16. *Photographs of fabricated pressure sensor array: (a) A side-view of the pressure sensor array; (b) a close-up view of the gap (approximately 44 μm) defined between electroplated nickel backplate and pressure sensitive Kapton flexible plate.*

Measurement

The capacitance of individual pressure sensors has been measured using a Keithley 3322 LCZ meter. Measured capacitances for undeflected pressure sensors were in the range from 11.35 pF to 13.97 pF depending on the length of interconnections between bonding pads and sensors. It has been observed that capacitance monotonically increases with increasing applied pressure, meaning that the pressure sensitive Kapton plate deflects toward the fixed backplates. Over an applied pressure range from 0 to 34 kPa, the net capacitance change was approximately 0.14 pF. Theoretical prediction of the sensor behavior is determined by taking the first three terms of equation (6) (i.e., up to n=2). Theoretical and measured net capacitance change over the applied pressure range are compared in Figure 17. Theoretical data shown in Figure 17 is based on an initial gap (d_1) of 40 μm. There is approximately a 10~20 % difference between the measured physical gap and the 40 μm gap value used to provide a best fit between theory and experiment. This difference could be explained by the fringing effects of the sensor capacitance (since the flexible plate is circular and the backplate is a square the side length of which exceeds the diameter of the flexible plate). The measured values of relative capacitance change are in the range from 1 - 1.34 %.

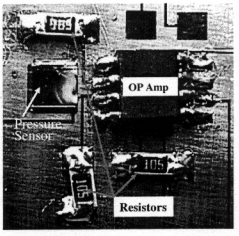

Figure 18. *Frequency-to-voltage circuitry integrated with four sensors on the underside of the array.*

An OP-amp-based astable multivibrator circuit has been integrated with the pressure sensors in a hybrid fashion (Figure 18) to create a frequency-modulated voltage output. The capacitance of the pressure sensor is the frequency-determining capacitance, which modulates the frequency of the voltage output on the output of the amplifier. Figure 19 shows the frequency output of the OP-amp circuit as a function of applied pressure from 0 to 30 kPa. The measured value of relative frequency change is 0.93 % over the applied pressure range from 0 to 30 kPa.

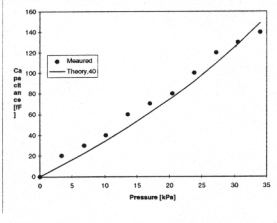

Figure 17. *A comparison of theoretical and measured values of net capacitance change over the full range of applied pressure ranging from 0 to 34 kPa.*

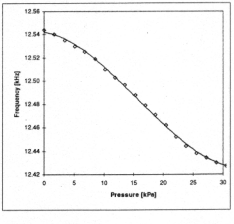

Figure 19. *Frequency output of the hybrid multivibrator circuit in response to pressure sensor capacitance change over the applied pressure ranging from 0 to 30 kPa.*

Summary - Pressure Sensors

Robust materials have been studied as suitable substrates for micromachined devices. Lamination using a hot press, combined with traditional micromachining processes, has been investigated as a suitable fabrication process for the robust substrates. A capacitive pressure sensor array using a robust substrate (0.5mm thick stainless steel shim stock), Kapton HN200 flexible plate, and lamination processing has been designed, fabricated, and characterized. Over the applied pressure range from 0 to 34kPa, the net capacitance change of the pressure sensor is approximately 0.14 pF. OP-amp-based multivibrator circuitry has been integrated with pressure sensors in a hybrid manner to create frequency-modulated outputs. A physical demonstration of a surface-mount chip directly integrated on laminated Kapton polyimide film has been performed to show the feasibility of parasitic capacitance elimination for higher sensitivity.

STAINLESS STEEL MODULATORS FOR MICROMACHINED SYNTHETIC JETS

The use of synthetic jets [7] as fluidic actuators enables the possibility of altering the apparent aerodynamic shape of an airfoil by creating a closed recirculation region without extending any mechanical parts into the crossflow of the airfoil. This approach is very suitable for a MEMS-based flow control scheme, since (1) such devices have already been demonstrated as being compatible with micromachining technology [8]; and (2) the relatively 'delicate' MEMS devices do not need to be exposed to the flow; in fact, the devices can be recessed under an orifice plate, safely out of reach of the flow. A microjet, pressure sensor, and provision for integrated circuitry can also be combined together to form a module suitable for repetition into an array. Such a module contains a modulator to switch the synthetic jets on and off at each orifice hole, a pressure sensor to sense the local pressure, and some local electronics to perform readout, signal linearization, and/or local control. This section focuses on the development of robust modulators for synthetic jet actuators.

A robust microjet modulator array has been fabricated using stainless steel as a substrate, Kapton film as an insulator, and thin stainless steel foil (50 μm thick) as the modulator material. Microjet drivers have been assembled with these robust modulators and the velocity profiles of the MEMS-modulated synthetic jets for multiple numbers of modulators in an array has been measured using particle image velocimetry (PIV). The modulators operate by electrostatically opening and closing a plate which bears an array of holes and which covers the orifice plate. When the plate is in contact with the substrate, the substrate orifice hole is blocked and the synthetic jet cannot issue from the orifice. When the plate is not in contact with the substrate, the synthetic jet can flow through the holes in the orifice plate and through the orifice hole in the substrate, thereby allowing a synthetic jet to issue from the orifice hole.

The fabrication sequence of the robust modulator array is shown in Figure 20. The process starts on square 5.7 cm (2 inch) on a side, 0.5 mm (20 mil.) thick stainless steel substrates. An array of 5x5 orifice holes with a diameter of 2 mm, with 10 mm center-to-center distances, are milled through the substrate. Kapton film (Dupont, Kapton HN200, 50μm [2 mil.] thick) is laminated onto the milled stainless steel using a hot press. Stainless steel foil (50 μm [2 mil.] thick: AISI-T302) is laminated again on top of the Kapton polyimide film using a hot press. Photoresist SC1813 (Shipley) is spun onto the laminated stainless steel foil. Photoresists are photo-defined and the stainless steel metal foil is wet etched. The modulation actuators will thus be formed by the stainless steel foil in the regions suspended over the milled orifice holes. The Kapton film has been isotropically dry etched using a barrel plasma etcher. Finally, a 5.6 μm thick parylene film is conformally deposited for electrical insulation. Figure 21 shows a photomicrograph of an array of fabricated modulators.

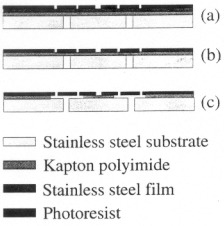

Figure 20. *Fabrication sequence of robust modulator.*

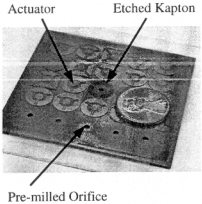

Figure 21. *Fabricated stainless steel modulators. Note that the central modulator has been intentionally removed to show the orifice hole.*

After the fabrication of an array of robust modulator, the modulator array has been assembled with microjet drivers (Figure 22). Both electromagnetic and piezoelectric drivers have been assembled and tested. The assembled robust modulator/jet driver has been tested using particle image velocimetry (PIV). Figure 23 shows raster plots of the velocity magnitude for three modulators with different diameter vent holes (the vent holes of the modulator at 10 mm [x-axis] is the largest and the one at 30 mm is the smallest) with all modulators open. This PIV test result shows that the robust modulator/jet driver can create jets with centerline speeds at y/d≈10 (where d is the diameter of the orifice hole) of as much as 6 m/s.

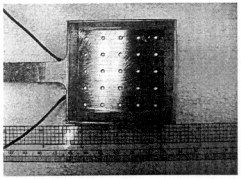

Figure 22. *An array of robust modulators assembled with a central microjet driver, showing the array of orifice holes. This all-stainless view is what the external crossflow 'sees'.*

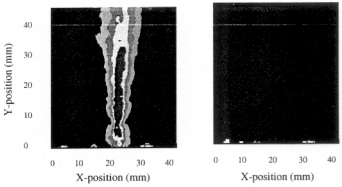

Figure 23. *Velocity profile (PIV data) for three modulators in the array. Left: central modulator open; others closed; right: all closed. The maximum velocity shown is 6 m/s.*

CONCLUSIONS

The advantages of MEMS technology, namely batch fabrication, integration with electronics, large arrays of elements, and fine feature sizes, can be combined with robust materials to produce sensors and actuators with extended operating parameters over silicon. Three examples are given in this paper; hopefully, many others will be exploited by the aeronautics and astronautics community in the near future.

ACKNOLEDGEMENTS

Portions of this work were supported by AFOSR, DARPA, and ARO. In addition to the authors, this paper represents a review of the work of the gollowing Georgia Tech graduate students and postdoctoral associates: Dr. J.B. Lee, Mr. Sung-Pil Chang, Mr. Brian English, Mr. Christopher Rinehart, Dr. Martin von Arx, and Ms. Jennifer English, and they are gratefully acknowledged.

REFERENCES

1. G. Blasquez, P.Pons, and A. Boukabache, "Capabilities and limits of silicon pressure sensors", *Sensors and Actuators*, vol. 17, pp. 387-403.

2. R. Okojie, A. Ned, D. Kurtz, and W. Carr, "6H-SiC pressure sensors for high temperature applications", Proc. MEMS 1996, pp. 146-149.

3. E. Obermermeier, "High Temperature microsensors based on polycrystalline diamond thin films", Proc. International Conf. Transducers '95, pp. 178-181, 1995.

4. Dupont Applied Technologies Group, "Green Tape Material System, Design and Layout Guidelines", pp. 1-17.

5. A. Sedra and K. Smith, Microelectronic Circuits, Saunders College Publishing, 1991, pp. 786-788.

6. S. Timoshenko, Theory of Plates and Shells, McGraw-Hill, 1940.

7. R. D. James, J. W. Jacob, and A. Glezer, "A round turbulent jet produced by an oscillating diaphragm," *Journal of Physics of Fluids*, vol. 8, no. 9, pp. 2482-2495, 1996.

8. D. J. Coe, M.G. Allen, M.A. Trautman, and A. Glezer, "Micromachined jets for manipulation of macro flows" in *Proceedings 1994 Solid-State Sensors and Actuators Workshop*, Hilton Head, SC, 1994, pp.243-247.